Journal of Energy Storage 114 (2025) 115800

Contents lists available at ScienceDirect

Journal of Energy Storage

journal homepage: www.elsevier.com/locate/est

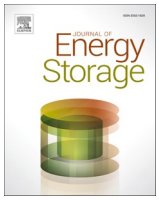

Research Papers

Comparative analysis of different Rankine PTES system configurations

Mario Petrollese [a,*], Matteo Marchionni [a], Rosa P. Merchán [b], Luca Migliari [a], Giorgio Cau [a]

[a] Department of Mechanical, Chemical and Materials Engineering, University of Cagliari, Via Marengo, 2, 09123 Cagliari, Italy
[b] Department of Applied Physics and Institute of Fundamental Physics and Mathematics (IUFFYM), University of Salamanca, 37008 Salamanca, Spain

ARTICLE INFO

Keywords:
Energy storage
Pumped thermal energy storage
Organic Rankine cycle
Exergy analysis

ABSTRACT

In this paper, four main configurations of a Rankine-based Pumped Thermal Energy Storage (PTES) system are proposed and compared in terms of achievable electrical and exergy roundtrip efficiency and energy density. The analysis considers a conventional setup employing commercial heat pumps and Organic Rankine Cycle (ORC) systems integrated with a Thermal Energy Storage (TES) unit as reference. The initial findings indicate that off-the-shelf systems result in roundtrip efficiencies lower than 40%, even under optimal high-temperature conditions at the heat pump evaporator inlet. This is primarily due to significant exogenous exergy destructions inherent in the commercial equipment. The study then explores upgraded alternatives to the reference PTES configuration, focusing on optimizing the heat pump layout and selecting non-conventional working fluids. This optimization process includes evaluating various working fluids, where n-hexane is identified as the optimal choice for achieving the highest electrical and exergy roundtrip efficiencies, particularly at evaporator inlet temperatures above 60°C. For lower temperature ranges, acetone emerges as a more suitable fluid due to its favorable thermodynamic properties. Further enhancements are made by optimizing the ORC layout, specifically through the introduction of an additional thermal storage tank and improved heat exchangers. These modifications are aimed at minimizing heat transfer losses and thereby boosting the overall system performance. With these changes, the PTES system's roundtrip efficiency reaches approximately 70%.

The most advanced configuration integrates the heat pump and ORC systems into a single assembly, utilizing the working fluid not only for energy transfer but also as a storage medium. This integration reduces the number of required components and further increases efficiency. As a result, roundtrip efficiencies of about 80% are achieved, representing a significant advancement over current commercial systems.

1. Introduction

The global shift towards Renewable Energy Sources (RES), such as solar and wind, has seen significant growth in recent years. However, despite increased investments in electrification, energy efficiency, and additional renewable capacity, fossil fuels still supply more than 60 % of global electricity demand [1]. The International Energy Agency estimates that achieving Net Zero Emissions by 2050 will require tripling the current installed RES capacity by 2030 [2–6]. This rapid expansion poses significant challenges for grid management and stability [7]. In this context, energy storage technologies will play a critical role in balancing electricity demand with the intermittent supply from RES. Storage systems will need to operate in the short, medium, and long term to facilitate a greater penetration of RES into the energy mix, enabling a smoother transition towards a decarbonized economy [8,9]. For short and medium-term applications, electro-chemical energy storage systems, also known as Battery Energy Storage System (BESS), have a competitive advantage, thanks to their high roundtrip efficiency, superior energy density and fast response time. However, the need of critical raw materials, the strong dependency of operating life from the number of charging/discharging cycles, and the high self-discharging rate limit their suitability for the wide range of services required by grids characterized by high-RES penetration [10] Consequently, there is a need to develop alternative energy storage technologies that could complement these types of storage systems. Chemical storage systems based on the power-to-hydrogen or power-to-liquid concept are promising but lack technological maturity [11] and the low roundtrip efficiency [12] still represents a strong barrier to their widespread adoption.

An attractive alternative are the Carnot batteries, a type of energy storage that uses thermodynamic cycles to store electrical energy as heat during charging and convert it back to electricity during discharging phase. Carnot batteries include technologies such as Pumped Thermal Energy Storage (PTES) systems. The latter use a Heat Pump (HP)

* Corresponding author.
E-mail address: mario.petrollese@unica.it (M. Petrollese).

https://doi.org/10.1016/j.est.2025.115800
Received 27 September 2024; Received in revised form 22 December 2024; Accepted 9 February 2025
Available online 18 February 2025

Nomenclature

Abbreviations

CH	Charge
CMP	Compressor
COND	Condenser
DIS	Discharge
EV	Evaporator
EX	Exergy
G	Generator
HP	Heat pump
HT	High temperature
IHX	Internal heat exchanger
LT	Low temperature
M	Motor
MT	Medium temperature
PHX	Pre-heater
PMP	Pump
RT	Roundtrip
SC	Sub-cooler
TRB	Turbine
TV	Throttling valve
WF	Working fluid

Acronyms

ORC	Organic Rankine Cycle
PTES	Pumped Thermal Energy Storage
RES	Renewable Energy Sources
TES	Thermal Energy Storage
TRL	Technology Readiness Level

Greek symbols

η	efficiency, [−]
ρ_E	energy density, [kWh/m^3]

Symbols

COP	Coefficient of Performance, [−]
e	specific exergy, [kJ/kg]
$\dot{E}$	exergy rate, [kW]
$\dot{E}_D$	exergy destruction rate, [kW]
$\dot{m}$	mass flow rate, [kg/s]
$\dot{Q}$	heat flow, [kW]
t	time, [h]
T	temperature, [°C]
V	volume, [m^3]
W	electrical energy, [kWh]
$\dot{W}$	work rate, [kW]

tipically powered by excess or low-cost grid electricity to transfer heat from a low-temperature reservoir to a high-temperature one, storing energy as heat in a Thermal Energy Storage (TES) system. During discharge, the stored heat is converted back into electricity using a heat engine, providing power during periods of high demand or high electricity prices [13].

PTES systems can store energy with high roundtrip efficiency and low self-discharge rates. Moreover, their lifetime is independent of the number of charging/discharging cycles [14,15]. Compared to Pumped-Hydro Energy Storage (PHES) systems, which currently account for over 96% of the global energy storage capacity [16], PTES systems have a smaller footprint, lower water usage, and do not require specific morphological conditions for their installation [17,18]. Moreover, when integrated with external low-temperature heat sources [19–21] —RES or waste industrial heat — their roundtrip efficiency can significantly increase [22]. Indeed, this is a very favorable feature, as it allows the utilization of unused energy sources and makes such systems suitable for multi-vector energy storage applications, which are considered critical for sector coupling and the energy transition [23]. Depending on the thermodynamic cycle and working fluid employed, PTES systems can be classified as Brayton PTES, which are based on the Joule-Brayton thermodynamic cycle and typically use air or argon as working fluid [24–26], transcritical PTES, which are based on a transcritical Rankine cycle that usually uses CO_2 as working fluid, and Rankine PTES systems, which are based on the Rankine cycle and use steam or organic fluids as working fluids [27]. Rankine PTES systems are more suitable for low-grade heat recovery [28] and, since they typically operate at lower temperatures (100–250°C), they can be more compact and cost-effective compared to other PTES concepts [26]. However, more research is required to make Rankine PTES competitive with other storage solutions [28], from both a technical and economical point of view, and especially when considering high operating temperatures and high operating temperature lifts for the heat pump. In light of this, the literature includes several studies on improving performance of Rankine PTES systems through layout modifications [14], different types of working fluids [29,30], or incorporation of technological advanced components [31–33]. Among them, particularly interesting are the studies performed in the framework of the CHESTER project [25], which employs, separately, a high temperature HP and an ORC system using R1233zd(e) as working fluid and being capable of storing both sensible and latent heat. The outcomes lay the framework for further development of the technology, whose performance and economic viability can be optimized by investigating and testing novel layouts and different types of working fluids.

As for the latter aspect, many works in the literature identify R1233zd(E), R1234ze(Z) and R245fa as optimal fluids [34,35], especially for the HP, as these fluids allow for the maximization of the HP Coefficient of Performance (COP), which can even reach a value of 4 [34]. Steger et al. [36] simulated and designed a pilot HP-ORC plant, selecting the R1233zd(E) as the best fluid regarding performance, cost and safety and obtaining a roundtrip efficiency of 59%. This pilot plant is operational, and first experimental tests are being conducted [37]. Such a result shows the promising potential of this technology, especially considering that several aspects of the research have not been addressed yet. Although various system configurations have been proposed in the literature, none has yet emerged as the optimal solution, highlighting a significant research gap in the field. Therefore, further analyses are needed to improve system layouts and enhance overall efficiency. To address this objective, this research investigates several alternative configurations for conventional Rankine-based PTES systems. Specifically, three Rankine PTES configurations are proposed and compared to a reference configuration consisting of commercially available components. One configuration minimizes the irreversibility occurring during the heat transfer between the TES system, the ORC system, and the heat pump. Another configuration reduces irreversibility in both the heat pump and the ORC system by eliminating one throttling valve and one pump. A further element of novelty is the consideration of several working fluids to evaluate their impact on the performance of the proposed configurations. The electrical roundtrip efficiency, the exergy efficiency and the energy density of the system are assessed for all the configurations. Among the optimization parameters are also considered different working fluids as well as the temperature of the water utilized at the beginning of the charging cycle. The effect on the system performance and on the exergy destruction rates at a component level is calculated and discussed. This research provides valuable insights for designing more efficient PTES units, helping to close the performance gap with more conventional energy storage solutions.

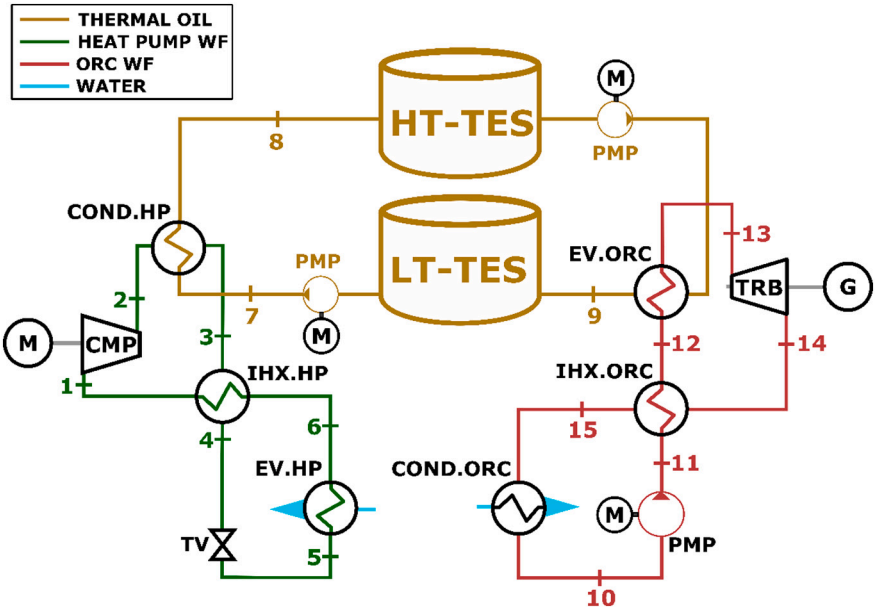

Fig. 1. Plant layout of the configuration A of the Rankine PTES system.

2. System configuration

The four Rankine PTES configurations herein considered include three main sections: a heat pump, a heat engine based on a ORC system and a thermal energy storage section. The latter consists of two (or three) storage tanks, at Low, Medium and High Temperature (LT-TES, MT-TES, HT-TES), which store thermal oil used both as heat transfer fluid and storage medium, along with two pumps. These pumps enable the circulation of a heat transfer fluid to transfer the thermal power supplied by the heat pump to the ORC system. To introduce flexibility to the energy storage system, the thermal oil pumps, the compressor of the heat pump and the ORC pump are coupled with inverter-driven electrical motors. Regardless of the configuration, the PTES system is characterized by a discharge power of 15 kW and a nominal discharge time of 4 h, while the design temperature of the HT-TES is set at 140°C. Moreover, a variable temperature at the evaporator inlet side is considered in the analysis. This allows to simulate the performance of the heat pump under different operating conditions, representing real scenarios where the system can be integrated with external heat sources (i.e. geothermal or a solar thermal).

As mentioned, four alternative configurations are examined:

- *Configuration A*: the HP and ORC systems are based on commercial products, available on the market, and the TES section includes two storage tanks (LT-TES and HT-TES)
- *Configuration B*: the same ORC system of configuration A is considered, while the design of the HP is optimized.
- *Configuration C*: both the HP and the ORC system designs are optimized, and an additional storage tank (MT-TES) is introduced.
- *Configuration D:* the HP and the ORC systems are integrated into a unique system with the inclusion of an extra storage section for the working fluid.

In the following subsections, each configuration is described in detail and graphically represented through a simplified scheme, along with the thermodynamic diagrams of the HP cycle and the ORC cycle at design conditions. In the simplified schemes and thermodynamic diagrams, the green colour represents the charging circuit, the red colour represents the discharging circuit and the orange colour represents the TES section.

2.1. Configuration A

The reference system configuration, herein referred to as A, is shown in Fig. 1. As previously stated, this configuration is based on a commercial high temperature HP - based on a reverse Rankine cycle - and a commercial ORC system [38]. During the charging phase, the heat pump raises the temperature of the heat transfer fluid stored in the LT-TES, which is subsequently stored in the HT-TES. During the discharge phase, the heat transfer fluid stored in the HT-TES is used as a heat source for the ORC system. Both the ORC system and the heat pump use the same fluid, R1233zd(E), which is selected for its very low greenhouse effect, non-flammability, and absence of impact on ozone depletion. A minimum temperature difference in the heat exchangers of 10°C and a subcooling of the working fluid at HP condenser (COND.HP) of 5°C are assumed. As an example, Fig. 2 shows the T-s diagrams and T-Q diagrams of the heat pump and ORC system in case of a water temperature at the evaporator heat pump equal to 100°C.

2.2. Configuration B

Configuration B includes the same commercial ORC system of configuration A and a customized HP. The plant layout of this configuration is shown in Fig. 3. As can be observed, an additional heat exchanger within the HP, namely a sub-cooler (SC), is included to increase the sub-cooling of the organic fluid leaving the condenser. The SC allows to improve the heat transfer between the thermal oil and the working fluid at the liquid phase, with a consequent increase in the effectiveness of the heat exchange, and to reduce the irreversibility.

Indeed, as shown in Fig. 4(a-b), with respect to configuration A, configuration B achieves a reduction in the average temperature differences between the working fluid and the thermal oil. Moreover, a decrease in the average temperature difference between hot and cold streams in the internal heat exchanger (IHX.HP) and a reduction in temperature drop in the throttling valve (TV) also occurs, leading to a reduction in the HP exergy destruction.

2.3. Configuration C

In the configuration C (Fig. 5), in addition to the optimization of the HP design, the design of the ORC system is also optimized, with the aim of maximizing the roundtrip efficiency of the PTES system. The

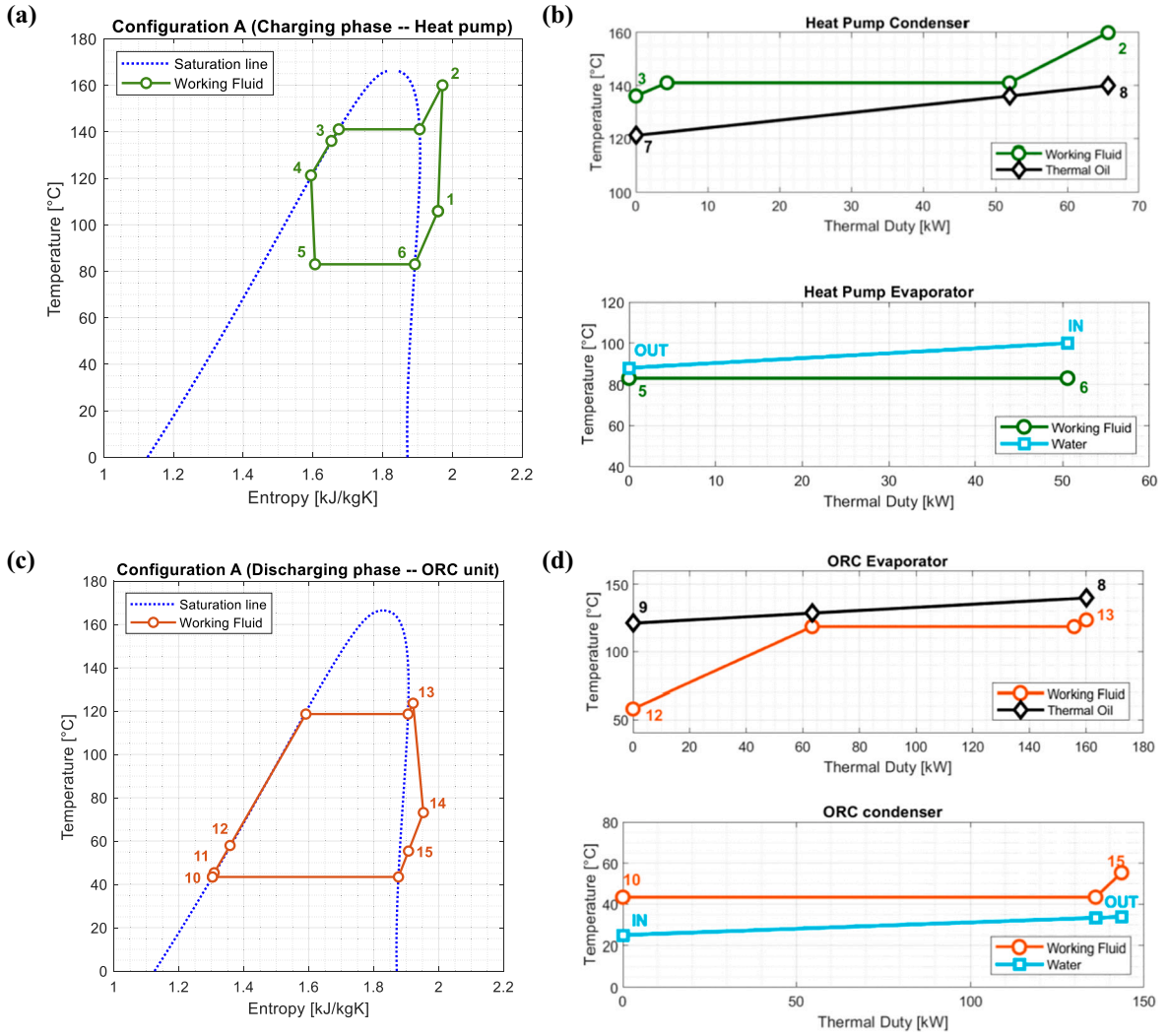

Fig. 2. Configuration A: T-s diagram (a) and T-Q diagram (b) for the heat pump (charging phase) and T-s diagram (c) and T-Q diagram (d) for the ORC system (discharging phase).

minimum temperature difference within these components is lowered from 10°C to 5°C by increasing their heat transfer area to reduce the exergy destruction occurring in the heat exchangers. A dedicated heat exchanger for preheating the organic fluid is introduced in the ORC system layout. The aim of this solution is to optimize the heat transfer in the pre-heater (PHX) and evaporator (EV.ORC) by lowering the thermal oil mass flow rate circulating in the pre-heater with respect to that circulating in the evaporator, consequently improving the thermal match between the thermal oil and the organic working fluid in both heat exchangers. Therefore, this arrangement leads to a reduction in exergy losses and an enhancement of the overall performance of the PTES storage system. To implement this arrangement, a three-way valve and an additional thermal storage tank are included to split the thermal oil flow rate coming from the high-temperature thermal storage tank (HT-TES). An additional thermal storage tank (MT-TES) is added to the scheme to operate at a temperature which is intermediate between the ones of the HT-TES and LT-TES tanks. Clearly, a proper modification of the HP layout with the introduction of a three-way valve upstream of the sub-cooler SC is also required. This valve allows to keep the same temperature level at the intermediate MT-TES and to operate with a ratio between mass flow rate circulating in the HP sub-cooler ($\dot{m}_{SC}$) and that circulating in the condenser ($\dot{m}_{COND.HP}$) equal to the ratio between the flow rate circulating in the ORC pre-heater ($\dot{m}_{PHX}$) and in the subsequent evaporator ($\dot{m}_{EV.ORC}$). The changes introduced in the heat transfer process between TES section and HP/ORC can be seen in Fig. 6.

2.4. Configuration D

In configuration D both the HP and the ORC system are merged in a single assembly, as shown in Fig. 7. This arrangement allows to reduce the number of system components but requires two additional storage tanks to store the working fluid at the beginning of the charging and discharging cycle. A minimum temperature difference of 10°C is considered across the heat exchangers. The part of the circuit depicted in green in Fig. 7 represents the HP in the other three configurations, operating during the charging stage. The one highlighted in red operates during the discharging phase, assuming the role of the ORC system. The working fluid is initially stored in a low temperature (LT) refrigerant tank. During the charging phase, the refrigerant is pressurized by the pump (PMP) and vaporized in the low-temperature evaporator (LT EV) thanks to the high temperature water. Once vaporized and superheated, the working fluid is compressed by the compressor (CMP), subsequently condensed in the high-temperature condenser (HT COND) and stored in the high-temperature refrigerant tank as saturated liquid. The thermal energy released by the condensation of the working fluid is recovered by a stream of thermal oil, which flows from the low-temperature TES tank

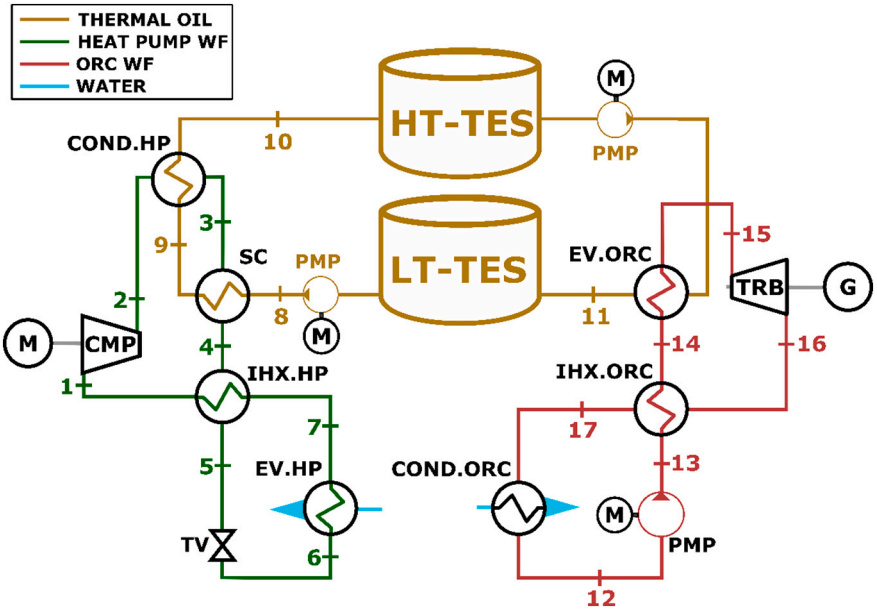

Fig. 3. Plant layout of the configuration B of the Rankine PTES system.

(LT-TES) into the high-temperature TES tank (HT-TES), at a temperature of 140°C.

During the discharging phase, the saturated liquid is slightly expanded in the throttling valve (TV). Although the throttling valve introduces dissipation, it is necessary to perform the system's discharging process and to re-convert the electricity absorbed during the charging stage. At the end of the charging process, assuming negligible thermal losses, without throttling, the working fluid would have a temperature higher than that of the heat transfer fluid used in the TES system. This is evident in Fig. 8(b), where the temperature at point 4 is higher than that of the thermal oil (point "Oil_{IN}" in Fig. 8(b)). Consequently, during the discharging phase, the evaporation of the working fluid would not occur completely due to the reduced temperature difference across the heat exchanger.

By throttling the working fluid—slightly lowering its pressure and, consequently, its temperature (points 6 in Fig. 8(c-d)) it becomes possible to utilize the thermal energy stored during the charging stage, thereby enabling its conversion back to electricity. In fact, the organic fluid is vaporized and superheated in the high-temperature evaporator (HT EV) thanks to the thermal energy coming from the thermal oil stream flowing from the HT-TES to the LT-TES tank. In this process, the temperature of the thermal oil decreased from 140°C to roughly 120°C. After being evaporated, the working fluid expands in the turbine (TRB) producing mechanical energy which is consequently converted into electricity by the generator (G). After the expansion, the working fluid is condensed in the low temperature condenser (LT COND) and stored back in the LT refrigerant tank.

3. System modelling

The models for the four Rankine PTES configurations have been developed using MATLAB software [39]. Thermophysical properties of water and organic fluids have been obtained from CoolProp [40] while Therminol SP has been considered as thermal oil [41]. For both HP and ORC models, temperature, pressure, specific entropy and specific enthalpy of each point have been calculated by establishing mass flow and enthalpy balances and considering pump, compressor and turbine isentropic efficiencies. Pressure drops and heat losses through components and pipes, which are secondary losses, have been neglected. The maximum temperature reached during the charging cycle (outlet of the compressor, CMP) has been limited to 160°C, as recommended by Hassan et al. [42].

The exergy of each subsystem has been also computed to analyze the exergy efficiency and the exergy losses at component level. The classical exergy rate balance equation at steady state has been implemented for each component, as follows:

$$\sum \dot{m}_i e_i + \dot{Q}\left(1 - \frac{T_a}{T_c}\right) = \sum \dot{m}_o e_o + \dot{W} + \dot{E}_D \tag{1}$$

where $\dot{m}$ is the mass flow rate of the stream substance, $\dot{Q}$ is the heat flow through component boundary, T_a is the ambient temperature, T_c is the temperature at component boundary at which heat is exchanged with the environment, e is the specific exergy of the stream (based on the system configuration only the physical exergy defines the total specific exergy of such streams), $\dot{W}$ is the work rate of the component, and $\dot{E}_D$ is the exergy destruction in the component due to irreversibility. Subscripts i and o represent the inlet and outlet from the component, respectively.

To evaluate the performance of the PTES system, the electrical roundtrip efficiency, the exergy roundtrip efficiency and the energy density have been used. Specifically, the electrical roundtrip efficiency (η_{RT}) has been defined as the ratio between the electrical energy produced during the discharging cycle W_{DIS} (from the ORC in configurations A-C or by the turbine TRB in configuration D) and the one consumed during the charging cycle W_{CH} (by the heat pump in configurations A-C or by the compressor and the pump in configuration D). For configurations A, B and C, assuming that the heat pump and ORC always operate at nominal conditions, η_{RT} can be also computed as the multiplication of the Coefficient of Performance of the Heat Pump (COP_{HP}) by the efficiency of the ORC (η_{ORC}) and by the efficiency of the Thermal Energy Storage (η_{TES}) as described in Eq. (2). For configuration D, η_{RT} can be calculated as per Eq. (3)

$$\eta_{RT} = \frac{W_{DIS}}{W_{CH}} = \frac{\dot{W}_{ORC} \bullet t_{DIS}}{\dot{Q}_{EV.ORC} \bullet t_{DIS}} \bullet \frac{\dot{Q}_{EV.ORC} \bullet t_{DIS}}{\dot{Q}_{COND.HP} \bullet t_{CH}} \bullet \frac{\dot{Q}_{COND.HP} \bullet t_{CH}}{\dot{W}_{CMP} \bullet t_{CH}} = \eta_{ORC} \bullet \eta_{TES} \bullet COP_{HP} \tag{2}$$

$$\eta_{RT} = \frac{W_{DIS}}{W_{CH}} = \frac{\dot{W}_{TRB} \bullet t_{DIS}}{\dot{W}_{CMP} \bullet t_{CH} + \dot{W}_{PMP} \bullet t_{CH}} \tag{3}$$

where t_{DIS} and t_{CH} are the discharging and charging times, respectively.

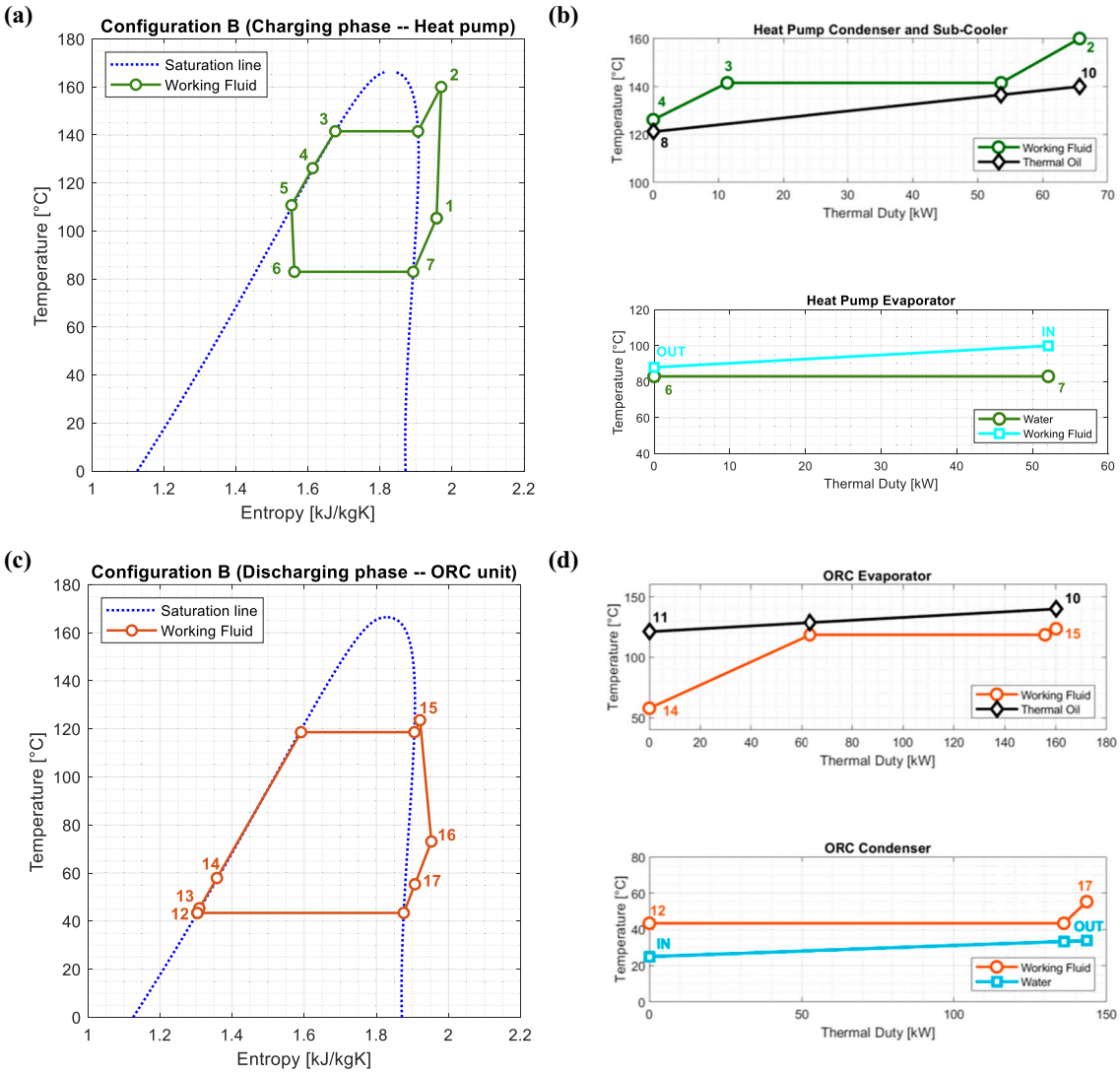

Fig. 4. Configuration B: T-s diagram (a) and T-Q diagram (b) for the heat pump (charging phase) and T-s diagram (c) and T-Q diagram (d) for the ORC system (discharging phase).

Instead, the exergy roundtrip efficiency ($\eta_{EX,RT}$) has been defined as the ratio of the overall exergy produced during the discharging cycle (from the ORC system in configurations A-C and from the part of the circuit highlighted in red in Fig. 7 for the configuration D) and the overall exergy introduced in the charging cycle (in the heat pump for configurations A-C and from the part of the circuit highlighted in green in Fig. 7 for the configuration D). Eq. (4) and Eq. (5) show the expression of the exergy efficiency for configurations A-C and configuration D, respectively. In Eq. (4), $\dot{E}_{EV.HP}$ and $\dot{E}_{COND.HP}$ represent the exergy flows entering the heat pump evaporator and condenser respectively, while $\dot{E}_{EV.ORC}$ stands for the exergy flow entering the ORC evaporator. In Eq. (5), $\dot{E}_{HT\ EV}$ and $\dot{E}_{HT\ COND}$ represent the exergy flows entering the high temperature evaporator and condenser, respectively, in configuration D.

$$\eta_{EX,RT} = \frac{\dot{W}_{ORC}}{\dot{E}_{EV.ORC}} \bullet \frac{\dot{E}_{EV.ORC} \bullet t_{DIS}}{\dot{E}_{COND.HP} \bullet t_{CH}} \bullet \frac{\dot{E}_{COND.HP}}{\dot{W}_{CMP} + \dot{E}_{EV.HP}} \tag{4}$$

$$\eta_{EX,RT} = \frac{\dot{W}_{TRB}}{\dot{E}_{HT\ EV}} \bullet \frac{\dot{E}_{HT\ EV} \bullet t_{DIS}}{\dot{E}_{HT\ COND} \bullet t_{CH}} \bullet \frac{\dot{E}_{HT\ COND}}{\dot{W}_{CMP} + \dot{E}_{HT\ EV}} \tag{5}$$

It is worth noting that the electrical roundtrip efficiency does not include the thermal energy supplied by the hot water to the heat pump, aligning with conventional metrics used for assessing the efficiency of electricity storage systems, while exergy roundtrip efficiency reflects the overall thermodynamic efficiency, incorporating both electrical and thermal contributions. This distinction between electrical and exergetic efficiencies aligns with methodologies proposed in the literature for analysing thermally integrated PTES systems [43,44].

Finally, the energy density of the PTES system, which represents the overall average energy stored per TES volume, has been defined as the ratio between the energy produced by the ORC system during a fully discharging phase and the sum of the internal volume of the various tanks introduced in the TES section (V_{tanks}):

$$\rho_E = \frac{W_{DIS}}{V_{tanks}} \tag{6}$$

4. Results and discussion

The expected performance of the proposed four Rankine PTES system configurations is discussed in this section. In particular, the electrical roundtrip efficiency, the exergy efficiency, the energy density and the exergy destruction for each configuration are assessed varying the water inlet temperature feeding the HP evaporator. Indeed, higher water temperatures allow to reduce the temperature rise of the working fluid

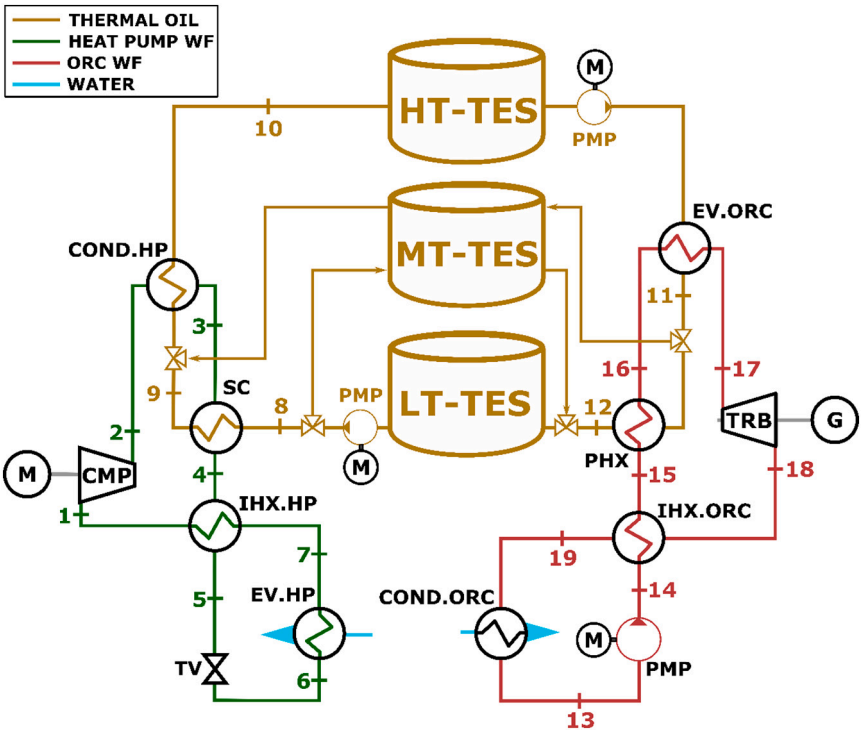

Fig. 5. Plant layout of the configuration C of the Rankine PTES system.

provided by the compressor during the charging cycle, and therefore to increase the overall storage system efficiency. Since configuration A is based on commercial components, only the R1233zd(E) fluid is considered in it, while for the other three configurations, the analysis is extended to include other fluids (cyclopentane, n-hexane, and acetone) to evaluate their impact on system performance.

For configuration C, the comparison of working fluids was also performed, but for the sake of simplicity, not all the results are shown. Therefore, only the results obtained for the optimal working fluid are reported, focusing the analysis instead on another key parameter affecting the layout performance, which is the ratio between the mass flow rate of working fluid circulating in the ORC pre-heater ($\dot{m}_{PHX}$) and the one circulating in the evaporator ($\dot{m}_{EV.ORC}$). Table 1 and Table 2 reports the main input parameters assumed for the four configurations.

4.1. Configuration A

To evaluate the expected performance of the system configuration based on commercial HP and ORC units, the technical data reported in the datasheets of commercial units [38] are used as a reference. The declared nominal efficiency of the ORC system is about 0.10 while the heat pump COP achieved with a temperature lift of 40°C (which means an inlet water temperature at EV.HP of 100°C) is about 4. Consequently, the electrical roundtrip efficiency of this PTES system is around 0.40.

To better characterize the system performance, an exergy analysis is carried out. As shown in Fig. 9(b), the main irreversibility of configuration A occurs in the turbomachines (CMP/TRB). However, reducing these endogenous exergy destructions is hindered by the current technological state-of-the-art. Significant irreversibility occurs also in the heat exchangers, especially in the evaporator of the ORC system. These losses can be reduced by decreasing the minimum allowed temperature (with a consequent increase in the heat transfer area) but since they are mainly exogenous, its minimization can be reached only by reducing the mean temperature difference. By assuming a water inlet temperature at the EV.HP of 100°C, electrical and exergy roundtrip efficiencies of about 0.40 and 0.25, respectively, are obtained, as shown in Fig. 9(a). Decreasing the water inlet temperature at EV.HP results in an increase in the temperature lift provided by the heat pump. Consequently, as shown in Fig. 9, this leads to increased exergy losses and degradation of the overall PTES performance, with a drop in the roundtrip and exergy efficiencies up to 0.21 and 0.19, respectively. This is mainly due to an increase of the exergy destruction in the throttling valve of the heat pump, which has to face an increasing pressure drop with the reduction of the water inlet temperature. In fact, a pressure ratio of about 3 is observed for a water inlet temperature at the EV.HP of 100°C, which increase up to about 10 with a water temperature of 60°C. As for the exergy destruction in the ORC section, it is approximately equally divided between evaporator, condenser and turbine. The variation of the water temperature at the EV.HP has no effect, since the inlet temperature of the water at the COND.ORC and of the thermal oil at the EV.ORC is constant.

Finally, the decrease in the temperature of the water entering the EV.HP also leads to a reduction in thermal power released at the condenser at the heat pump and, thus, in the charging times. However, no variations in the TES volumes and in the ORC energy delivery are expected resulting in a constant PTES energy density equal to about 0.45 kWh/m^3.

4.2. Configuration B

In configuration B, the ORC system is the same as that of configuration A, while the HP is customized by introducing a dedicated subcooler downstream of the condenser. Additional working fluids are considered, with respect to R1233zd(E), to investigate the possibility of further improving the HP performance. Specifically, in a preliminary screening step the selection space of the working fluid candidates is reduced to a group of organic fluids considering criteria as critical temperatures falling within the range of 150–245°C, low flammability, as well as Ozone Depletion Potential (ODP) and Global Warming Potential (GWP) lower than 5. Afterwards, a parametric analysis aimed at maximizing the COP by varying the inlet water temperature at the EV.HP has allowed to further reduce the list of suitable candidates. In this

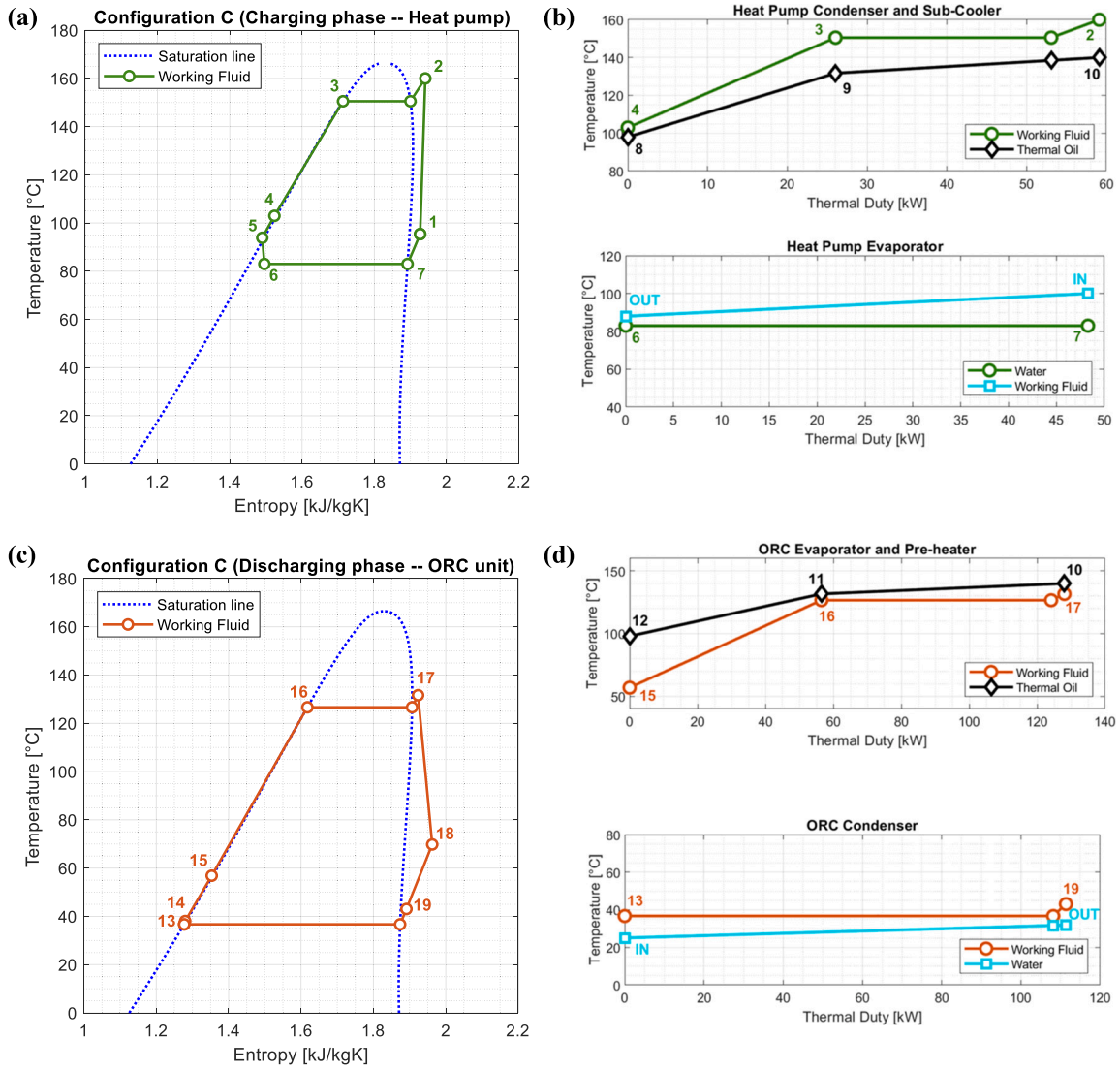

Fig. 6. Configuration C: T-s diagram (a) and T-Q diagram (b) for the heat pump (charging phase) and T-s diagram (c) and T-Q diagram (d) for the ORC system (discharging phase).

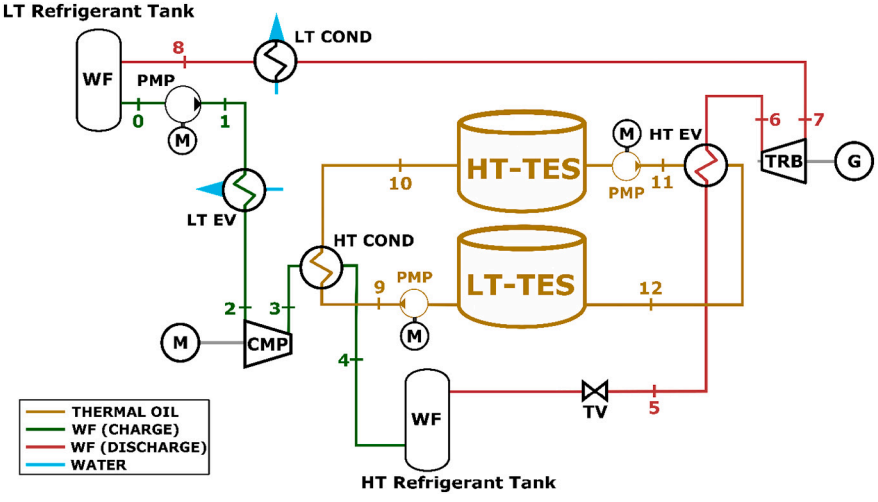

Fig. 7. Plant layout of the configuration D of the Rankine PTES system.

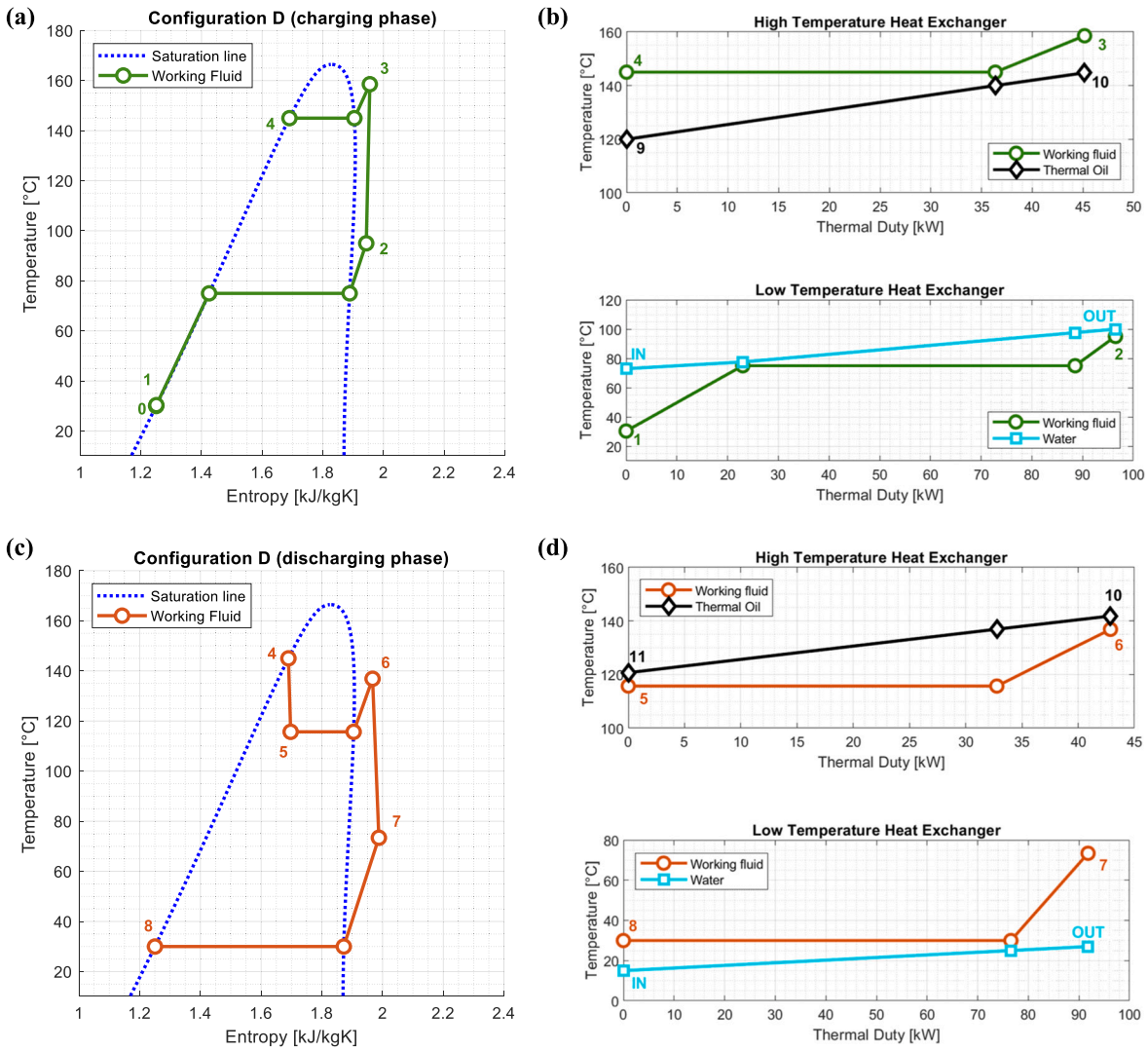

Fig. 8. Configuration D: T-s diagram (a) and T-Q diagram (b) for the charging phase and T-s diagram (c) and T-Q diagram (d) for the discharging phase.

Table 1
Assumptions for the turbomachines' efficiency.

Turbomachines	Pump (PMP)	Compressor (CMP)	Turbine (TRB)
Isentropic efficiency	0.6	0.8	0.7
Electro-mechanical efficiency	0.95		

Table 2
Assumption for the PTES layouts.

PTES system		
Power capacity during charge	[kW]	15
Power capacity during discharge	[kW]	15
Discharging time	[h]	4
TES system – Therminol SP®		
Thermal efficiency		0.98
Maximum operating temperature	[°C]	140
Minimum operating temperature	[°C]	120
Heat sink - Water		
Temperature at beginning of discharging phase	[°C]	25
Temperature at beginning of charging phase	[°C]	50–100

way, the rest of the study is performed with the 3 working fluids achieving the best performance: n-hexane, cyclopentane, and acetone. Additionally, R1233zd(E) is displayed in order to compare in a more straightforward way with configuration A. Fig. 10(a) shows the ones with the highest potential to maximize the roundtrip efficiencies of the storage system. In general, the alternative fluids achieve better performance compared to R1233zd(E), which is the fluid used in the commercial heat pump, leading to an increase of 3–6 percentage points in the electrical roundtrip efficiency. At evaporating temperatures higher than 60°C, n-hexane leads to the highest electrical roundtrip efficiency (maximum of 0.53 when the temperature at the EV HP reaches 100°C), while slightly lower performance is achieved by cyclopentane and acetone. On the other hand, acetone should be preferred below these temperatures although the performance improvement over that obtained by using n-hexane is marginal (less than 1 percentage point). Regarding the exergy roundtrip efficiency, a similar behavior compared to electrical roundtrip efficiency is found, but with larger differences among working fluids for low evaporator inlet temperatures (see Fig. 10 (b)). The highest exergy roundtrip efficiency (0.29) is also achieved by n-hexane when water inlet temperature at the HP evaporator reaches 100°C. On the other hand, the optimized performance of the HP pump does not affect the energy density of the PTES system, which remains equal to that obtained for configuration A.

To better understand the influence of the working fluids on PTES

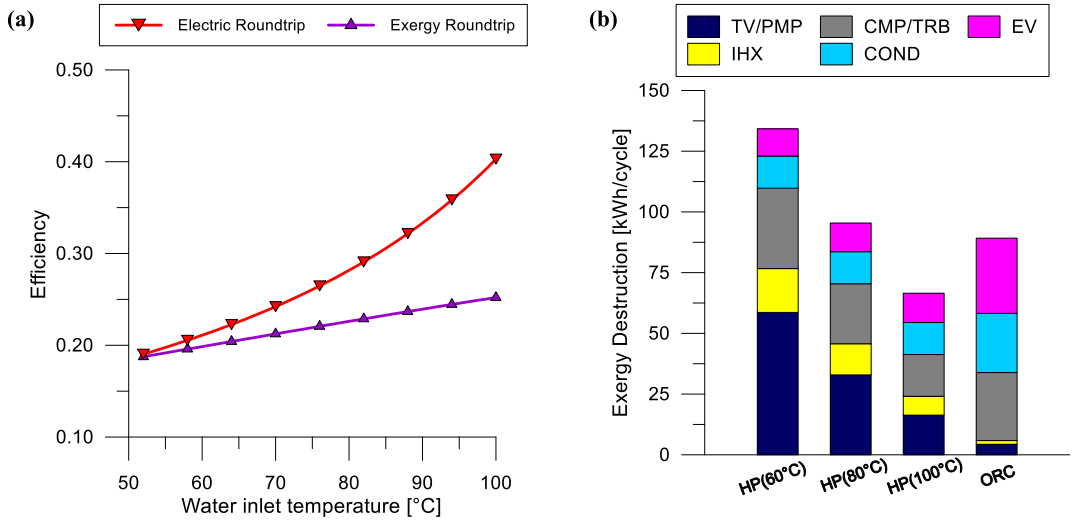

Fig. 9. Configuration A performance analysis varying the water temperature at the inlet of the heat pump evaporator: electrical roundtrip efficiency, exergy efficiency (a) and exergy destruction in the different components of the heat pump and ORC system during a complete charging/discharging cycle (b).

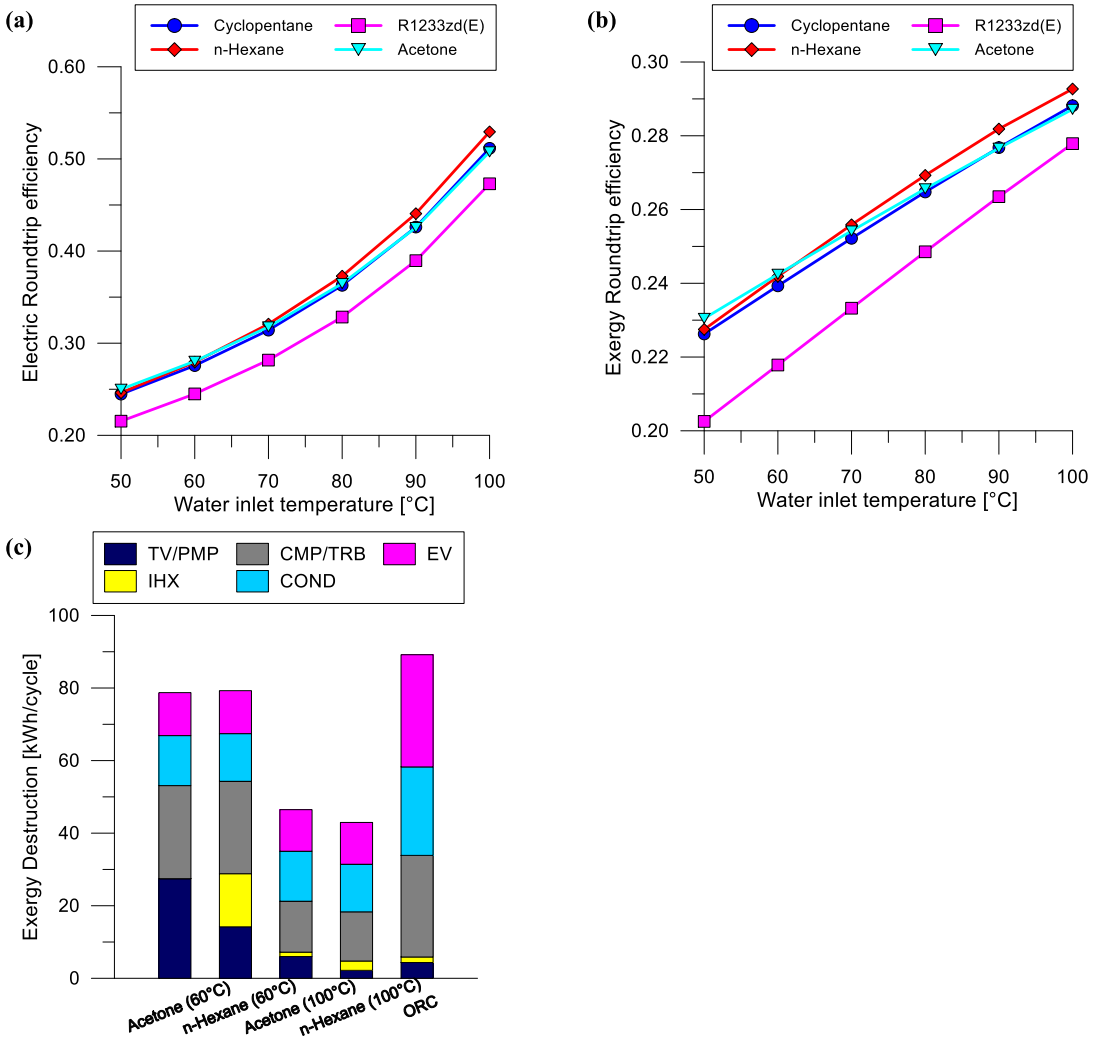

Fig. 10. Configuration B performance analysis varying the water temperature at the inlet of the heat pump evaporator and for different working fluids: electrical roundtrip efficiency (a), exergy roundtrip efficiency (b) and exergy destruction in the different components of the heat pump and ORC system during a complete charging/discharging cycle (c).

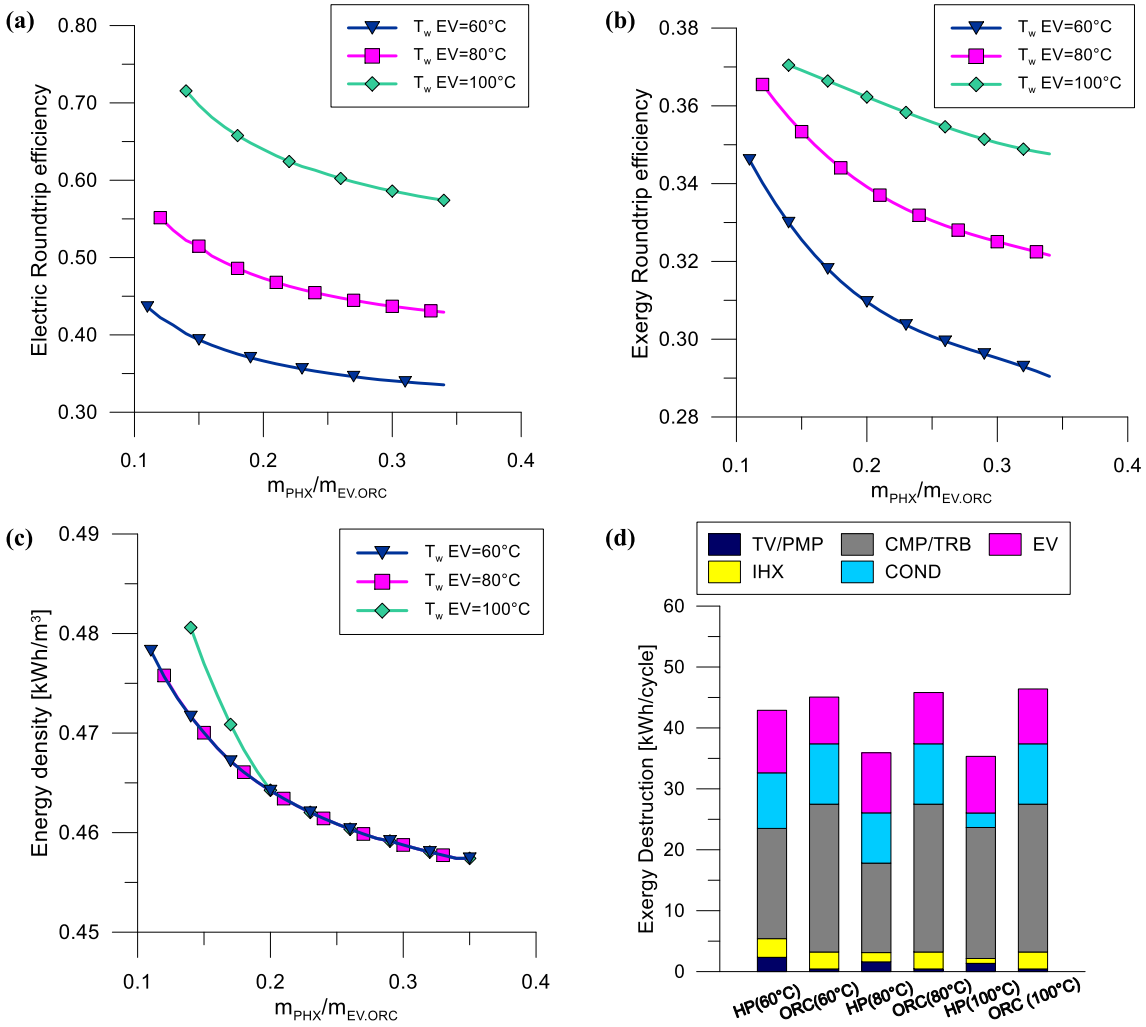

Fig. 11. Configuration C performance analysis varying the water temperature at the inlet of the heat pump evaporator and for different values of the ratio between the mass flow rates of working fluid flowing in the ORC pre-heater and evaporator: electrical roundtrip efficiency (a), exergy roundtrip efficiency (b), energy density (c) and exergy destruction in the different components of the heat pump and the ORC system during a complete charging/discharging cycle (d) (n-hexane is considered as working fluid).

performance, Fig. 10(c) compares the exergy destruction between acetone and n-hexane for temperatures at the HP evaporator inlet of 60°C and 100°C. Compared to configuration A, the reduction in the exergy losses in the TV and IHX are the main advantages. This is mainly due to the introduction of the sub-cooler downstream of the condenser, which decreases both the average temperature difference in the IHX and the fluid cooling occurring in the TV. By considering a water inlet temperature at the EV.HP of 60°C, the IHX is not introduced when acetone is used as working fluid resulting in a slightly lower exergy destruction compared to the use of n-hexane (78.7 kWh/cycle instead of 79.3 kWh/cycle). A general reduction in exergy destruction can be observed with higher evaporating temperatures, which allows to reduce the exergy losses in the compressor, internal heat exchanger and throttling valve. This reduction in the exergy destruction is mainly due to the decrease in the pressure ratio, as already observed for the configuration A. At an evaporator temperature of 100°C, the exergy destruction for the n-hexane case is about 3.5 kWh/cycle lower than that of acetone thanks to the lower irreversibility introduced in the TV. This is due to the specific shape of the saturation curve of the working fluid, which results in a higher internal heat recovery in the IHX for n-hexane and a consequent lower temperature at the TV inlet side for n-hexane compared to acetone.

4.3. Configuration C

For this configuration, the same working fluid candidates of configuration B are considered, but only the outcomes of the fluid with the best performance (n-hexane) are shown. As it can be seen in Fig. 11 (a), a further increase in the electrical roundtrip efficiency of about 15–20 percentage points compared to configuration B is achieved by using this system configuration and n-hexane as working fluid for both the HP and ORC system, reaching values higher than 0.70 for water temperature at EV.HP inlet side of 100°C and minimum allowed ratio between thermal oil circulating in ORC pre-heater and evaporator. In fact, the lower the ratio of the mass flow rates, the greater the increase in the electrical roundtrip efficiency. A similar trend is observed also for the exergy roundtrip efficiencies (Fig. 11(b)), with achieved values higher than 0.30 also by considering an evaporator inlet temperature of 60°C. However, the variation introduced in this index with the increase in ratio of the mass flow rates and the water temperature is reduced compared to that observed in the electric roundtrip efficiency.

This is mainly due to the increasing reduction of the average temperature difference between cold and hot flow during the preheating phase of the ORC working fluid, with a consequent decrease in the exergy losses in this component. This is confirmed by Fig. 11(d), where an important reduction in the exergy destroyed in the EV.ORC can be

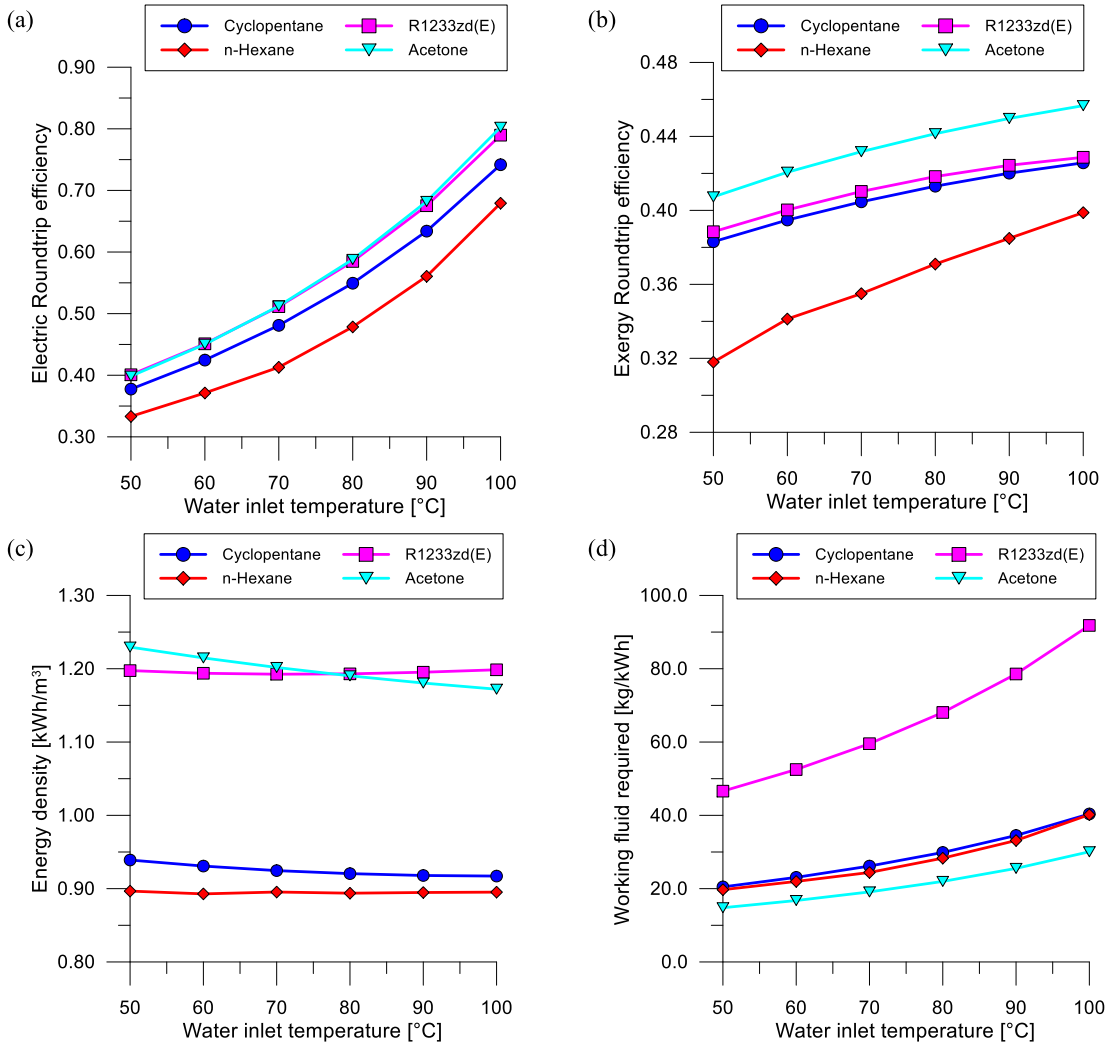

Fig. 12. Configuration D performance analysis varying the water temperature at the inlet of the low temperature evaporator and for different working fluids: electrical roundtrip efficiency (a), exergy efficiency (b), energy density (c) and the mass of working fluid required to store one kWh of electrical energy, namely working fluid utilization (d).

observed compared to previous configurations (about 9 kWh/cycle instead of 31 kWh/cycle obtained in configuration A). It should be noted that there is a minimum value of the ratio $\dot{m}_{PHX}/\dot{m}_{EV.ORC}$, in the range of 0.11–0.14, which occurs when the temperature difference at the ORC pre-heater between the incoming organic fluid and the outgoing heat transfer fluid reaches the minimum allowed value (5°C). The ratio between the mass flow rate circulating in the pre-heater and that circulating in the evaporator is also limited to a maximum value of about 0.35 due to the constraint in the maximum inlet temperature that is introduced in the compressor of the heat pump (160°C).

Finally, although the reduction of the ratio $\dot{m}_{PHX}/\dot{m}_{EV.ORC}$ involves the introduction of an increasingly larger MT-TES, the improvement in the ORC performances leads to a slight increase in energy density compared to configurations A and B. As can be observed in Fig. 11(c), this rise becomes more and more significant with the decrease of the mass flow rate circulating in the pre-heater/sub-cooler, thanks to the increase of the exergy content stored in the TES system.

4.4. Configuration D

The results related to configuration D are shown in Fig. 12. As can be observed, the layout allows to achieve higher electrical roundtrip efficiencies compared to the other configurations (Fig. 12(a)). In particular, the electrical roundtrip efficiency increases when the water temperature flowing at the inlet of the low temperature evaporator increases (Fig. 12 (a)). Higher water temperatures allow indeed to vaporize the fluid stored in the LT refrigerant tank at higher pressures, and therefore to shift part of the mechanical energy required to compress the fluid from the compressor to the pump, improving the overall efficiency of the process. Conversely, the reduced energy consumption translates in a lower energy storage capacity per kg of fluid processed, leading in a greater amount of refrigerant used and in a larger tank volume (Fig. 12 (a) and Fig. 12(d)). Therefore, the system energy density decreases with the increase of water temperature at the inlet of the evaporator (Fig. 12 (c)).

The maximum electrical roundtrip efficiency achievable from this layout is about 0.80, obtained using acetone as working fluid and considering a water temperature at the evaporator inlet equal to 100°C. In this case, the energy density of the PTES system is 1.2 kWh/m^3. Similar performance can be obtained using the R1233zd(E) fluid, which shows an electrical roundtrip efficiency of 0.79 and an energy density of 1.2 kWh/m^3 for a water temperature at the evaporator inlet of 100°C, which is also a more environmentally friendly fluid. PTES systems using R1233zd(E), however, would require a greater amount of working fluid to store a unit of energy (Fig. 8.d), implying higher cost per kWh of energy capacity installed. The other two fluids show instead lower

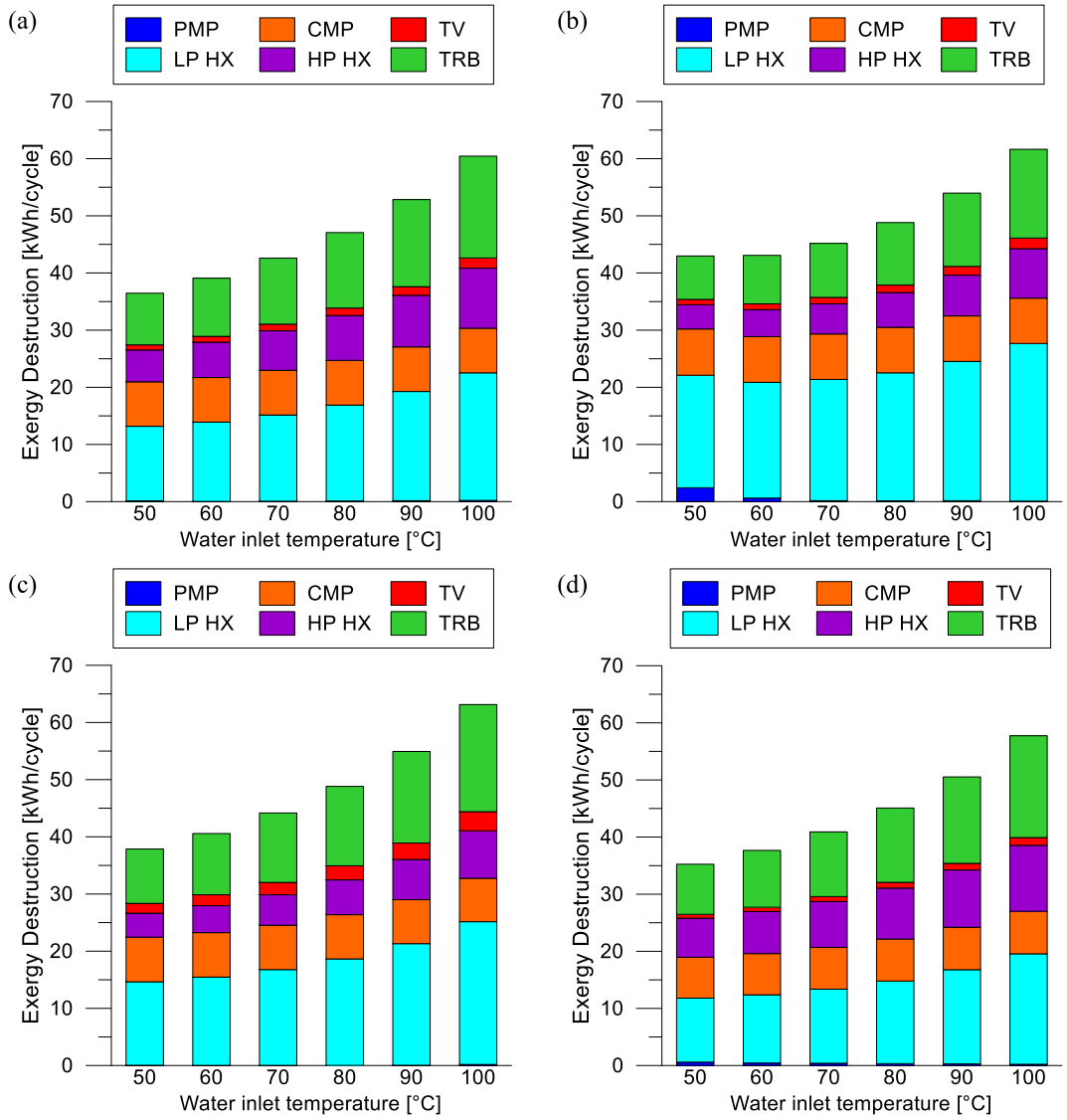

Fig. 13. Exergy destruction during a charging/discharging cycle for the different components embedded in the Configuration D as a function of the water temperature at the inlet of the low temperature evaporator and for different working fluids: cyclopentane (a), n-hexane (b), R1233zd(E) (c) and acetone (d).

roundtrip efficiencies, 0.74 and 0.68 for the cyclopentane and n-hexane respectively, and lower energy densities of approximately 0.9 kWh/m^3 (Fig. 12(a) and Fig. 12(c)).The exergy roundtrip efficiency (Fig. 12(b)) resembles the trends seen in the electrical roundtrip efficiency, with the acetone achieving a much higher exergy efficiency compared to the R1233zd(E) case. The use of R1233zd(E) leads indeed to higher mass flow rates processed and then to higher exergy losses in the different components of the system. Therefore, the results in general suggest that by fixing the maximum and minimum design pressure of the system, working fluids characterized by thermophysical properties that allow to reduce the mechanical power required in the compression lead to higher roundtrip and exergy efficiencies but also to larger storage volumes for the working fluid itself and for the thermal oil used in the TES system. Indeed, if the energy storage capacity is fixed, higher mass flow rates of fluids must be processed in the compressor to absorb the same amount of electrical power, leading to greater quantities of working fluid and of thermal oil needed to absorb the thermal energy at the compressor outlet.

Lastly, Fig. 13 shows the exergy destruction rate as a function of the water temperature at the low temperature evaporator inlet (LT EV) and for the different fluids employed. The exergy destructions occurring in the heat exchangers are grouped by operating temperature, divided in the low-temperature ones (LT HX) that include the low-temperature evaporator and condenser (LT EV and LT COND in Fig. 8 (a)), and the high-temperature ones (HT HX) that include the high-temperature condenser and evaporator (HT COND and HT EV in Fig. 8 (a)).

It can be observed that:

- The increase in the water temperature at the evaporator inlet leads to a rise of the exergy loss in the system despite the rise in electrical roundtrip efficiency. This is due to the lower pressure ratio across the compressor which leads to higher efficiencies, but lower mass flow rate processed to store the same amount of energy. The increased mass flow rate then implies higher losses across the components of the system.
- The share of irreversibility occurring in turbomachines and heat exchangers are comparable, and, as expected, an increase in the turbomachinery isentropic efficiency could be led to major improvements in the system overall performance.
- The n-hexane and R1233zd(E) in Fig. 13(b) and Fig. 13(c) show the higher exergy losses occurring in heat exchangers, amounting to 36.1 kWh/cycle (59% of the overall exergy destruction rate) and 33.2

Table 3
Comparison and summary of the four analyzed configurations.

Configuration		A	B	C	D
HP design		Commercial	Customized: +SC	Customized: +3-way valve)	Unique system: 2 extra storage tanks for WF
ORC design		Commercial	Commercial	Customized: +PHX + MT-TES and 3-way valve	
HP / ORC WF		R1233zd(E)	Different WFs looking for maximizing η_{RT}: cyclopentane, n-hexane, acetone, R1233zd(E)		
η_{RT}	$T_{HP.EV}$ = 100 °C	0.40	0.53 (n-hexane)	0.72 (n-hexane)	0.80 (acetone)
	$T_{HP.EV}$ = 60 °C	0.21	0.28 (acetone)	0.44 (n-hexane)	0.45 (acetone)
$\eta_{EX,RT}$	$T_{HP.EV}$ = 100 °C	0.25	0.29 (n-hexane)	0.37 (n-hexane)	0.46 (acetone)
	$T_{HP.EV}$ = 60 °C	0.19	0.24 (acetone)	0.35 (n-hexane)	0.42 (acetone)
ρ_E (kWh/m^3)	$T_{HP.EV}$ = 100 °C	0.45		0.48 (n-hexane)	1.20 (R1233zd(E))
	$T_{HP.EV}$ = 60 °C			0.48 (n-hexane)	1.23 (acetone)
Advantages		Configuration with the highest TRL	High TRL, improved performance obtained with few HP design changes	High flexibility, significant performance improvement compared to conf. A	Configuration achieving the best performance
Drawbacks		Very low performance	Obtained performance not comparable with other energy storage systems	Performance lower than conf. D, need of an additional TES tank	Low TRL, need of two additional storage systems, performance to be experimentally validated

kWh/cycle (53% of the overall exergy destruction rate) respectively for a water inlet temperature of 100°C. This suggests that the optimization of the heat transfer processes in systems employing such fluids will be more effective in terms of increasing the system performance.

- The throttling valve (TV) represents a small share of the overall system exergy loss for all the fluids considered.
- The irreversibility occurring in the turbine is much higher than the one in the compressor due to the largest pressure ratio across the component, suggesting that among the two machines the turbine should be optimized to achieve the higher performance benefit.

4.5. Comparison of configurations

A summary of the main features of the four Rankine PTES configurations together with a comparison in terms of electrical and exergy roundtrip efficiencies, energy density and advantages/drawbacks are reported in Table 3. The commercial configuration (configuration A) is optimal from a Technology Readiness Level (TRL) point of view since it already employs commercial components. When criteria for determining optimal configuration focus on roundtrip efficiency and energy density, configuration D stands out clearly as the best option; although, the amount of refrigerant needed is larger, which translates into expected higher capital costs.

5. Conclusions

This study introduced and evaluated the performance of three configurations of Rankine-based Pumped Thermal Energy Storage (PTES) systems, compared to a conventional setup utilizing commercial components. The conventional setup, employing commercial equipment, exhibited significant exogenous exergy destructions, resulting in electrical roundtrip efficiencies of less than 40%, even at high inlet temperatures to the heat pump evaporator. The alternative - upgraded - configurations demonstrated substantial improvements in reducing exergy destruction and enhancing roundtrip efficiency. When optimizing the heat pump, n-hexane resulted to be the working fluid that allows to reach both the highest electrical and exergy roundtrip efficiencies (up to 53% and 29%, respectively) when the inlet water temperature at the evaporator exceeds 60°C, while for lower temperature a wet fluid as acetone should be preferred. Electrical roundtrip efficiency close to 70% was achieved by optimizing the heat transfer between the TES and the ORC system. This was obtained by adding a TES tank at intermediate temperature and a dedicated pre-heater in the ORC layout. The most advanced configuration analyzed, obtained by merging in one single system the heat pump and the ORC, allowed to reach a roundtrip efficiency of 80% and higher energy densities, given the lower oil tank volumes required to store the thermal energy produced during the charging phase and the higher electric energy generated during discharge. The promising results, especially with reference to the last two configurations, enable further research on the economic aspects and off-design performance, providing a comprehensive evaluation of their practical applicability and cost-effectiveness.

CRediT authorship contribution statement

Mario Petrollese: Writing – original draft, Investigation, Conceptualization. **Matteo Marchionni:** Writing – original draft, Methodology, Conceptualization. **Rosa P. Merchán:** Writing – original draft, Visualization, Formal analysis. **Luca Migliari:** Writing – review & editing, Writing – original draft, Validation, Methodology, Formal analysis. **Giorgio Cau:** Writing – review & editing, Supervision, Formal analysis.

Declaration of competing interest

The authors declare that they have no known competing financial interests or personal relationships that could have appeared to influence the work reported in this paper.

Acknowledgements

R. P. Merchán acknowledges a postdoctoral contract co-financed by the European NextGenerationEU fund, Spanish “Plan de Recuperación, Transformación y Resiliencia” fund, Spanish Ministry of Universities, and Universidad de Salamanca (“Ayudas para la recualificación del sistema universitario español 2021-2023: Margarita Salas”).

L.Migliari acknowledges the research project founded under the National Recovery and Resilience Plan (NRRP), Mission 4 Component 2 Investment 1.3 - Call for tender No. 1561 of 11.10.2022 of Ministero dell'Università e della Ricerca (MUR); funded by the European Union – NextGenerationEU. Project code PE0000021, Concession Decree No. 1561 of 11.10.2022 adopted by Ministero dell'Università e della Ricerca (MUR), CUP F53C22000770007, according to attachment E of Decree No. 1561/2022, Project title “Network 4 Energy Sustainable Transition –

NEST".

Data availability

Data will be made available on request.

References

[1] International Energy Agency (IEA), World Energy Outlook 2023, 2023.
[2] International Energy Agency (IEA), Net Zero by 2050 - A Roadmap for the Global Energy Sector, 2021.
[3] International Energy Agency (IEA), Renewable Energy Market Update - June 2023, 2023.
[4] International Energy Agency (IEA), World Energy Investment 2023, 2023.
[5] International Energy Agency (IEA), World Energy Outlook 2022, 2022.
[6] International Renewable Energy Agency (IRENA), Electricity Storage Valuation Framework: Assessing System Value and Ensuring Project Viability, 2020.
[7] V. Arabzadeh, R. Frank, Creating a renewable energy-powered energy system: extreme scenarios and novel solutions for large-scale renewable power integration, Appl. Energy (2024) 374, https://doi.org/10.1016/j.apenergy.2024.124088.
[8] M. Petrollese, D. Cocco, L. Migliari, G. Cau, Techno-economic analysis of a hybrid CSP-CPV power plant, in: ECOS 2016 - Proceedings of the 29th International Conference on Efficiency, Cost, Optimisation, Simulation and Environmental Impact of Energy Systems, 2016.
[9] L. Migliari, D. Micheletto, D. Cocco, Performance analysis of a diabatic compressed air energy storage system fueled with green hydrogen, Energies 16 (2023) 7023, https://doi.org/10.3390/EN16207023.
[10] A.R. Dehghani-Sanij, E. Tharumalingam, M.B. Dusseault, R. Fraser, Study of energy storage systems and environmental challenges of batteries, Renew. Sust. Energ. Rev. 104 (2019) 192–208, https://doi.org/10.1016/J.RSER.2019.01.023.
[11] G. Herz, C. Rix, E. Jacobasch, N. Müller, E. Reichelt, M. Jahn, et al., Economic assessment of power-to-liquid processes – influence of electrolysis technology and operating conditions, Appl. Energy 292 (2021) 116655, https://doi.org/10.1016/J.APENERGY.2021.116655.
[12] F. Lonis, V. Tola, G. Cau, Performance assessment of integrated energy systems for the production of renewable hydrogen energy carriers, E3S Web of Conferences 197 (2020) 01007, https://doi.org/10.1051/E3SCONF/202019701007.
[13] A. Benato, A. Stoppato, Pumped thermal electricity storage: a technology overview, Thermal Science and Engineering Progress 6 (2018) 301–315, https://doi.org/10.1016/J.TSEP.2018.01.017.
[14] W. Tian, H. Xi, Comparative analysis and optimization of pumped thermal energy storage systems based on different power cycles, Energy Convers. Manag. 259 (2022) 115581, https://doi.org/10.1016/J.ENCONMAN.2022.115581.
[15] A.M. Rabi, J. Radulovic, J.M. Buick, Pumped thermal energy storage technology (PTES): review, Thermo 3 (2023) 396–411, https://doi.org/10.3390/THERMO3030024.
[16] World Energy Council, Energy Storage Monitor - Latest Trends in Energy Storage - 2019, 2019.
[17] I. Vorushylo, P. Keatley, N. Shah, R. Green, N. Hewitt, How heat pumps and thermal energy storage can be used to manage wind power: a study of Ireland, Energy 157 (2018) 539–549, https://doi.org/10.1016/J.ENERGY.2018.03.001.
[18] J. Martinek, J. Jorgenson, J.D. McTigue, On the operational characteristics and economic value of pumped thermal energy storage, J. Energy Storage 52 (2022) 105005, https://doi.org/10.1016/J.EST.2022.105005.
[19] G.F. Frate, L. Ferrari, P. Sdringola, U. Desideri, A. Sciacovelli, Thermally integrated pumped thermal energy storage for multi-energy districts: integrated modelling, assessment and comparison with batteries, J. Energy Storage 61 (2023) 106734, https://doi.org/10.1016/J.EST.2023.106734.
[20] O. Dumont, V. Lemort, Mapping of performance of pumped thermal energy storage (Carnot battery) using waste heat recovery, Energy (2020) 211, https://doi.org/10.1016/j.energy.2020.118963.
[21] B. Kurşun, K. Ökten, Comprehensive energy, exergy, and economic analysis of the scenario of supplementing pumped thermal energy storage (PTES) with a concentrated photovoltaic thermal system, Energy Convers. Manag. 260 (2022) 115592, https://doi.org/10.1016/J.ENCONMAN.2022.115592.
[22] M.H. Nozari, M. Yaghoubi, K. Jafarpur, G.A. Mansoori, Development of dynamic energy storage hub concept: a comprehensive literature review of multi storage systems, J. Energy Storage 48 (2022) 103972, https://doi.org/10.1016/J.EST.2022.103972.
[23] R.B. Peterson, A concept for storing utility-scale electrical energy in the form of latent heat, Energy 36 (2011) 6098–6109, https://doi.org/10.1016/J.ENERGY.2011.08.003.
[24] M. Petrollese, M. Cascetta, V. Tola, D. Cocco, G. Cau, Pumped thermal energy storage systems integrated with a concentrating solar power section: conceptual design and performance evaluation, Energy 247 (2022) 123516, https://doi.org/10.1016/J.ENERGY.2022.123516.
[25] CHESTER - Compressed heat energy storage for energy from renewable sources: the project 2018. https://www.chester-project.eu/ (accessed April 5, 2023).
[26] A.V. Olympios, J.D. McTigue, P. Farres-Antunez, A. Tafone, A. Romagnoli, Y. Li, et al., Progress and prospects of thermo-mechanical energy storage-a critical review, Progress in Energy (2020) 3, https://doi.org/10.1088/2516-1083/abdbba.
[27] J. Mitali, S. Dhinakaran, A.A. Mohamad, Energy storage systems: a review, Energy Storage and Saving 1 (2022) 166–216, https://doi.org/10.1016/J.ENSS.2022.07.002.
[28] L. Migliari, M. Petrollese, G. Cau, D. Cocco, Techno-economic assessment and grid impact of Thermally-Integrated Pumped Thermal Energy Storage (TI-PTES) systems coupled with photovoltaic plants for small-scale applications, J. Energy Storage 77 (2024) 109898, https://doi.org/10.1016/J.EST.2023.109898.
[29] O. Dumont, V. Lemort, Pumped Thermal Energy Storage Based on ORC. Encyclopedia of Energy Storage, Elsevier, 2022, pp. 68–78, https://doi.org/10.1016/b978-0-12-819723-3.00087-1.
[30] D. Tillmanns, D. Pell, J. Schilling, A. Bardow, The thermo-economic potential of ORC-based pumped-thermal electricity storage: insights from the integrated design of processes and working fluids, Energ. Technol. (2022) 10, https://doi.org/10.1002/ENTE.202200182.
[31] B. Eppinger, D. Steger, C. Regensburger, J. Karl, E. Schlücker, S. Will, Carnot battery: simulation and design of a reversible heat pump-organic Rankine cycle pilot plant, Appl. Energy (2021) 288, https://doi.org/10.1016/J.APENERGY.2021.116650.
[32] G.F. Frate, L. Ferrari, U. Desideri, Rankine carnot batteries with the integration of thermal energy sources: a review, Energies 13 (2020) 4766, https://doi.org/10.3390/EN13184766.
[33] O. Dumont, G.F. Frate, A. Pillai, S. Lecompte, De paepe M, Lemort V., Carnot battery technology: a state-of-the-art review, J. Energy Storage 32 (2020) 101756, https://doi.org/10.1016/J.EST.2020.101756.
[34] O. Dumont, A. Charalampidis, V. Lemort, Experimental investigation of a thermally integrated carnot battery using a reversible heat pump/organic rankine cycle, in: International Refrigeration and Air Conditioning Conference, 2021.
[35] A.H. Hassan, J.M. Corberán, M. Ramirez, F. Trebilcock-Kelly, J. Payá, A high-temperature heat pump for compressed heat energy storage applications: design, modeling, and performance, Energy Rep. 8 (2022) 10833–10848, https://doi.org/10.1016/J.EGYR.2022.08.201.
[36] D. Steger, C. Regensburger, B. Eppinger, S. Will, J. Karl, E. Schlücker, Design aspects of a reversible heat pump - organic rankine cycle pilot plant for energy storage, Energy 208 (2020) 118216, https://doi.org/10.1016/J.ENERGY.2020.118216.
[37] D. Steger, J. Karl, E. Schlücker, Launch and first experimental results of a reversible heat pump-ORC pilot plant as Carnot battery, in: 6th International Seminar on ORC Power Systems, Munich (Germany), 2021.
[38] Rank. Rank® Organic Rankine Cycle equipment, modules and systems n.d. https://www.rank-orc.com/es/ (accessed April 19, 2023).
[39] The MathWorks Inc., MATLAB Version: (R2023a) Update 3, 2023.
[40] I.H. Bell, J. Wronski, S. Quoilin, V. Lemort, Pure and pseudo-pure fluid thermophysical property evaluation and the open-source thermophysical property library CoolProp, Ind. Eng. Chem. Res. 53 (2014) 2498–2508, https://doi.org/10.1021/ie4033999.
[41] Eastman. Therminol SP Heat Transfer Fluid | Therminol | Eastman n.d. https://www.therminol.com/product/71093454?pn=Therminol-SP-Heat-Transfer-Fluid (accessed April 19, 2023).
[42] A.H. Hassan, L. O'Donoghue, V. Sánchez-Canales, J.M. Corberán, J. Payá, H. Jockenhöfer, Thermodynamic analysis of high-temperature pumped thermal energy storage systems: refrigerant selection, performance and limitations, Energy Rep. 6 (2020) 147–159, https://doi.org/10.1016/J.EGYR.2020.05.010.
[43] S.S.M. Shamsi, S. Barberis, S. Maccarini, A. Traverso, Thermo-economic performance evaluation of thermally integrated Carnot battery(TI-PTES) for freely available heat sources, J. Energy Storage 97 (2024) 112979, https://doi.org/10.1016/J.EST.2024.112979.
[44] G.F. Frate, M. Antonelli, U. Desideri, A novel Pumped Thermal Electricity Storage (PTES) system with thermal integration, Appl. Therm. Eng. 121 (2017) 1051–1058, https://doi.org/10.1016/J.APPLTHERMALENG.2017.04.127.